Hole transport through proton-irradiated *p*-type silicon wafers during electrochemical anodization

M. B. H. Breese,[1] F. J. T. Champeaux,[1] E. J. Teo,[2] A. A. Bettiol,[1] and D. J. Blackwood[2]

[1]*Physics Department, National University of Singapore, Lower Kent Ridge Road, 119260 Singapore*

[2]*Materials Science & Engineering Department, National University of Singapore, Lower Kent Ridge Road, 119260 Singapore*

The hole current density flowing through and around proton-irradiated areas of *p*-type silicon during electrochemical anodization is simulated and studied experimentally using scanning electron microscopy and photoluminescence imaging. It is shown that for certain irradiation geometries the current flow may be either reduced or enhanced in areas adjacent to irradiated lines, resulting in enhanced or reduced rates of porous silicon formation and corresponding changes in photoluminescence intensity and feature height. The current flow to the surface is unaffected by both the beam straggle and the high defect density at the end of ion range, enabling feature dimensions of ~200 nm to be attained. This study has enabled fabrication of micromachined and patterned porous silicon structures in anodized wafers with accurate control of feature dimensions, layer thickness, and photoluminescence emission wavelength and intensity.

PACS number(s): 61.80.Jh, 42.82.Cr, 78.67.−n, 82.80.Fk

I. INTRODUCTION

Porous silicon (PSi) is of interest due to its photoluminescence (PL) and electroluminescence properties,[1–4] raising the possibility of producing light-emitting devices made of PSi with microelectronics compatibility.[5] The commonly observed red-orange PL band is centered around 1.4–1.9 eV (600–800 nm) and probably arises from quantum confinement effects produced by the low dimensionality of the silicon skeleton remaining after anodization.

A potentially important application of PSi is the production of combined optical and electronic devices incorporating patterned porous material directly onto a single-crystal Si substrate with a high spatial resolution. To this end there have been several studies of ion irradiation as a means of influencing PSi formation, all using low-energy, heavy ions where thin porous layers (~1 μm) were produced.[6–10] The use of focused MeV ion beams in a nuclear microprobe[11,12] to fabricate patterned PSi layers many microns thick with micron lateral resolution has recently been demonstrated.[13–15] Typically a focused 2-MeV proton beam is scanned over the wafer surface [Fig. 1(a)]. The beam loses energy as it penetrates the silicon and comes to rest at a well-defined range, equal to ~50 μm for 2-MeV protons in silicon. The stopping process damages the silicon lattice by producing additional defects which locally reduce the concentration of free charge carriers. By pausing the focused beam for different amounts of time at different locations, any pattern of localized damage can be built up. The irradiated wafer is then anodized in a dilute solution of hydrofluoric acid, by passing an electrical hole current through it with an applied bias, resulting in PSi formation at the surface [Fig. 1(b)].[16] The damaged regions inhibit this process, so a thinner, less porous layer is produced at the irradiated areas which emit light with different intensity or redshifted wavelength.[13–15]

After anodization, the porous silicon may be removed by immersion in potassium hydroxide (KOH), leaving a patterned surface structure which is a three-dimensional representation of the scanned pattern and dose [Fig. 1(c)]. Such direct surface patterning using accurately controlled doses of high-energy ion beams[17,18] has opened up new opportunities for the fabrication of a variety of high-aspect ratio, multi-level microstructures in silicon for optoelectronic and microelectromechanical systems (MEMS) applications.[19–22]

Many properties of PSi, such as emission intensity and wavelength, layer thickness, and porosity, are determined by the hole current density *J* flowing to the wafer surface during electrochemical anodization.[15,16] This paper uses simulations to study the fundamental processes influencing *J* in and around proton-irradiated regions during anodization, in order to better understand PSi formation for micromachining and light-emitting PSi applications.
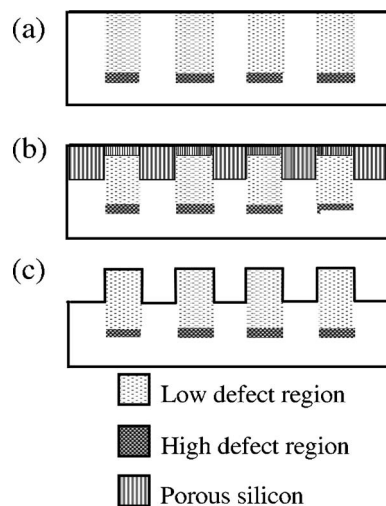

FIG. 1. (a) Patterning of *p*-type silicon with a focused MeV proton beam. (b) Patterned PSi formed after anodization. (c) Removal of porous silicon with diluted KOH.
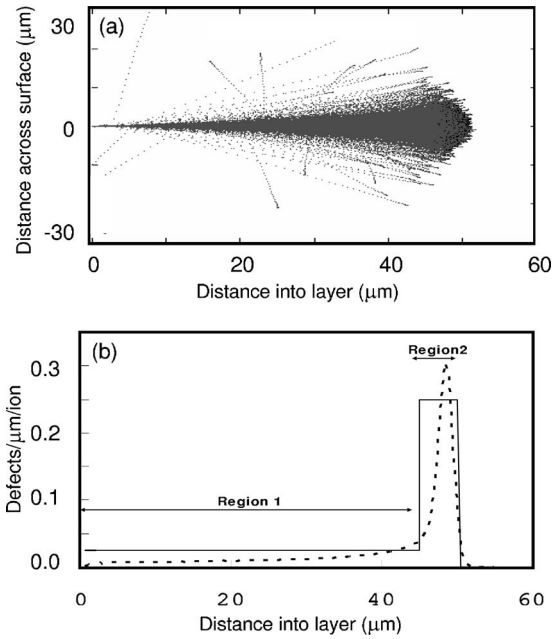
FIG. 2. (a). Trajectories of 10 000 2-MeV protons in silicon. Box size is 60×60 μm^2. (b) Number of defects created by 2-MeV protons in silicon (dashed line). The solid line shows the regions of low and high defect densities incorporated into MEDICI.

II. ION-INDUCED DEFECTS IN SILICON

Figure 2(a) shows trajectories of 2-MeV protons in silicon, obtained using the code SRIM (stopping and range of ions in matter).[23] SRIM uses a quantum-mechanical treatment of ion-atom collisions; the ion and atom have a screened Coulomb collision, including exchange and correlation interactions between the overlapping electron shells. Protons are deflected by many collisions with atomic electrons, resulting in an increase in beam spot size with depth. Ion irradiation of silicon introduces lattice damage as vacancy-interstitial pairs (Frenkel defects) along the ion trajectory. In Fig. 2(b), also obtained using SRIM, the number of Frenkel defects produced along the initial portion of the trajectories is fairly constant and then increases sharply towards the end-of-range. Many factors influence the resultant hole density in *p*-type silicon due to ion irradiation; defects may be stable or they may agglomerate into more stable divacancies and other vacancy- or impurity-related centers.[24–26] Electrically active defects act as trap levels in the energy band gap, where charge carriers undergo recombination through deep-level energy states, reducing the hole density and increasing the resistivity[27] of the irradiated region.

MEDICI (Ref. 28) models two-dimensional distributions of potential and carrier distributions in semiconductors by solving Poisson's equation and the electron and hole current continuity equations across the simulated region.[29] The solution methods used to solve the coupled nonlinear system formed by these equations are nonlinear iteration methods. Newton's method with Gaussian elimination of the Jacobian is considered more stable and has been used exclusively here. It can predict the electrical characteristics within the material for any applied bias conditions for a given distribution of specified defects. Defects are incorporated by defining their energy level in the band gap, their electron and hole trap lifetimes, and their relative concentrations. Table I shows the energy-level capture coefficients and relative concentrations, as determined in previous studies.[24–26,30] Five defect levels are specified: two electron traps and one hole trap are divacancy-related levels and have the same relative concentrations, the last hole trap and the last electron trap are impurity-related levels (carbon and oxygen). MEDICI uses trap lifetimes instead of capture coefficients to characterize each defect type, so τ_n and τ_p for each trap are calculated from Table I and the density of traps, N, using the relationship $\tau_{n,p} = 1/(N \times C_{n,p})$. No thermal annealing of defects at room temperature is assumed, and the total defect density given in Fig. 2(b) is incorporated into MEDICI in the ratios in Table I. Figure 2(b) shows the defect depth distribution incorporated in the MEDICI simulations as two uniform regions: a low-density region extends from the surface to a depth of 45 μm while a high-density region extends over a 5-μm depth beneath this, at the end-of-range.

In the following simulations, a beam of 2-MeV protons is used to irradiate 200-nm-wide, infinitely long lines and a current density of $J = 100$ mA/cm^2 is used during anodization, unless stated otherwise. The range of *p*-type wafer resistivity considered is $0.01 - 10$ Ω cm, typical of that used for producing light-emitting PSi.

Such simulations are shown to be useful in predicting the general behavior and form of the ion-irradiated structure after anodization, but should not be interpreted in a absolute manner, since they take no account of the time evolution of the anodization process or effects arising from conventional chemical etching.

TABLE I. Proton-induced defect traps incorporated into MEDICI.

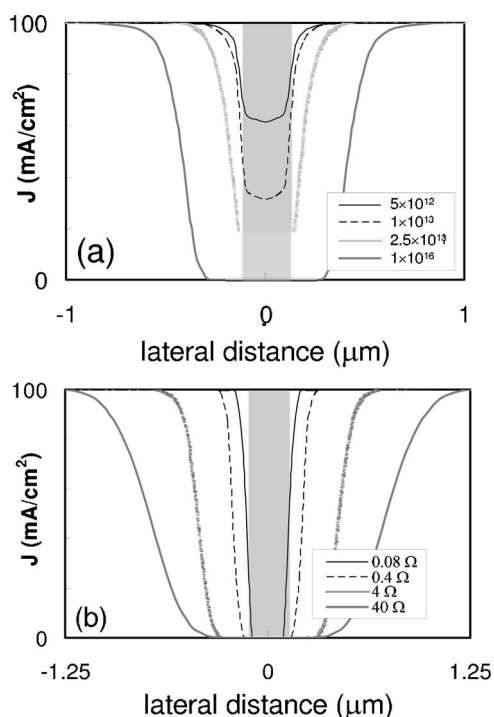| Defect	Trap energy, from midgap (eV)	Capture coefficients		Type	Relative concentration
		C_n (cm^3/s)	C_p (Cm^3/s)		
E_1	0.38	$(1.4 \times 10^{-8}) \times T^{0.5}$	$(8 \times 10^{-8})T^{0.7}$	Electron	3
E_2	0.33	$(1.6 \times 10^{-12}) \times T^{1.4}$	$(7 \times 10^{-7})T^{1.0}$	Electron	1
E_3	0.13	$(5.4 \times 10^{-9}) \times T^{0.4}$	$(2 \times 10^{-6})T^{0.3}$	Electron	1
E_4	−0.20	$(5.1 \times 10^{-23}) \times T^{5.2}$	$(1 \times 10^{-6})T^{0.61}$	Hole	1.5
E_5	−0.35	$\gg C_p(E_5)$	$(2.1 \times 10^{-9})T^{0.2}$	Hole	1

FIG. 3. MEDICI plots of J across a region containing a single irradiated line (gray area). The curves are normalized to the same J in the background for easier comparison. (a) A $3-\Omega$ cm wafer irradiated with different proton doses/cm^2. (b) Different resistivity wafers irradiated with a proton dose of 10^{16}/cm^2.

III. SINGLE-LINE IRRADIATIONS

Figure 3(a) plots J across a region of a $3-\Omega$ cm wafer containing a line irradiated with different proton doses. At low doses J through the irradiated line remains significant, so the line will be etched but at a lower rate than the unirradiated background. In this low-dose regime, J, and hence the physical and electronic properties of the PSi in the irradiated line, varies rapidly with dose. PSi with variable intensity and wavelength and variable height of machined features can be produced if accurate control over the dose is possible.[13,17] With increasing dose $(2.5 \times 10^{13}$/cm$^2)$ J reduces to zero across the irradiated line, so little or no PSi is expected. This dose results in micromachined areas corresponding to the original wafer surface and patterned PSi with areas emitting no PL.[17] At high doses $(10^{16}$/cm$^2)$ the regions over which J is zero, or reduced from its background level, are $\sim$300 nm and $\sim$500 nm, respectively, on each side of the irradiated line. Thus, above a certain dose the only effect of further irradiation is to widen the area over which PSi formation is reduced.

That an increasing ion dose causing more damage and a reduced etching rate of irradiated areas is well understood, whereas its influence on the etching behavior of adjacent areas is not. Figures 4(a)–4(d) show MEDICI plots of the **E**-field vectors present within the wafer for four proton doses. Away from the irradiated line, the **E**-field vectors are due only to the positive bias applied to the wafer during anodization. These are perpendicular to the surface, so J is uniform. The net charge within the irradiated line differs
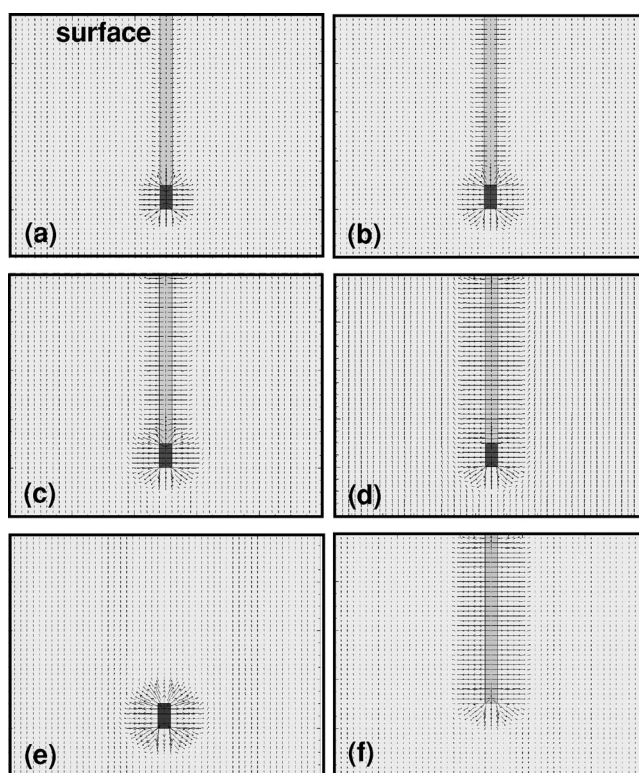

FIG. 4. MEDICI plots of **E**-field vectors present during anodization (logarithmic scale) in a region of a $3-\Omega$ cm wafer containing a line (gray area) irradiated with a dose of (a) 10^{11}/cm^2, (b) 10^{12}/cm^2, (c) 10^{13}/cm^2, and (d) 10^{14}/cm^2. The box sizes are 10 μm horizontally and 60 μm vertically. The dose in (e) and (f) is also 10^{14}/cm^2, but only the high- and low-defect-density regions are, respectively, considered.

from that of the unirradiated material because the hole capture coefficients are greater than the electron capture coefficients for four of the five defect trap levels present (see Table I). This gives a net positive charge to the irradiated regions, which is proportional to the defect density, producing an **E** field which is directed outwards. It extends farthest away from the irradiated line at the end-of-range and becomes stronger with increasing dose. This lateral **E** field is parallel to the surface and deflects holes away from the irradiated line, thus widening the region over which J is reduced in Fig. 3(a).

The high- and low-defect-density regions were separately simulated for a dose of 10^{14}/cm^2. The high-density region has no affect on J flowing to the surface of the irradiated line, which remains equal to the background level. Instead, J is only affected by the low-density region, which produces an effect indistinguishable from that of the full defect profile in Fig. 3(a). To explain this, only the high-density region is considered in Fig. 4(e), which results in a strong, localized distortion of the **E** field. However, at the surface the **E**-field vectors are perpendicular to it because the **E** field is only due to the applied bias, so J is unaffected. In Fig. 4(f), the **E**-field vectors around the low-density region are parallel to the surface, so the hole current is deflected away from the irradiated region, producing a decrease in J. This indicates that anodization of proton-irradiated areas is only influenced by the
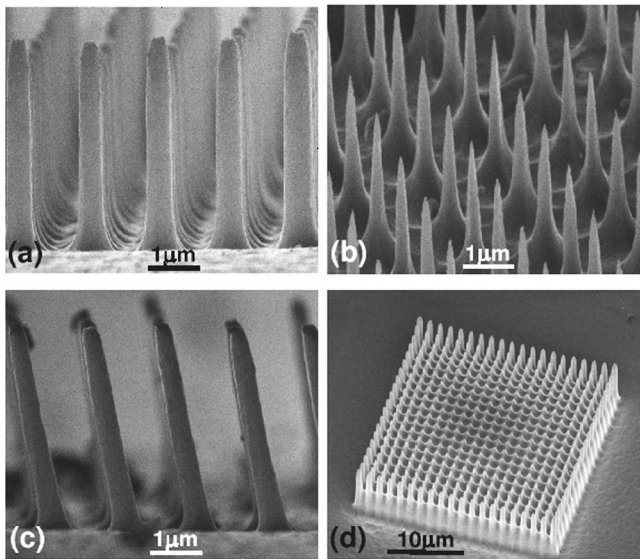
FIG. 5. SEM images of high-aspect-ratio pillars obtained by point irradiations with a 2-MeV proton dose of 5×10^{16}/cm^2 into a $3-\Omega$ cm wafer. The samples were then anodized for 15 min at J =40 mA/cm^2. (a) Beam perpendicular to surface and not aligned with a major crystal axis. (b) Beam axially channeled along surface-normal [001] axis. (c) Beam tilted 10° with respect to the perpendicular, not aligned with a major crystal axis. (d) Created under similar conditions as (a), but with smaller gaps between the point irradiations.

defect density at the surface rather than within the bulk. Hence the patterning process is not limited by the lateral beam straggle shown in Fig. 2(a), so one can achieve narrow lateral features if the correct irradiation dose is used.

Figure 5 shows a scanning electron microscope (SEM) image of arrays of high-aspect-ratio pillars produced by point irradiations. In Fig. 5(a) the proton beam was perpendicular to surface. The large dose completely stops the etching process, so the tops of the pillars correspond to the height of the original wafer surface. The pillars in Fig. 5(b) were produced under identical conditions except that the beam was axially channeled. Due to the lower defect density created close to the surface in channeling alignment,[31] the irradiated areas are significantly etched, resulting in sharp tips with radii of ~10 nm. In Fig. 5(c) an array of pillars similar to Fig. 5(a) was produced with the beam tilted by 10°. This is reproduced in the tilt of the pillars which shows that the etching process follows the direction of the low-density region. Neither of the structures in Figs. 5(b) and 5(c) would be created if the etching process was significantly influenced by the high-defect region.

Figure 3(b) plots J across a region containing a line irradiated with a high dose of 10^{16}/cm^2 for different resistivity wafers. The region over which J is reduced increases with wafer resistivity. This is because a given dose will result in a larger lateral **E** field in a higher-resistivity wafer since it gives a larger net charge to the irradiated area. Experimentally this makes it difficult to accurately control the optimum dose required to just reduce J to zero through an irradiated line in higher-resistivity wafers, so narrow features are easier to produce in lower-resistivity wafers, as demonstrated below.
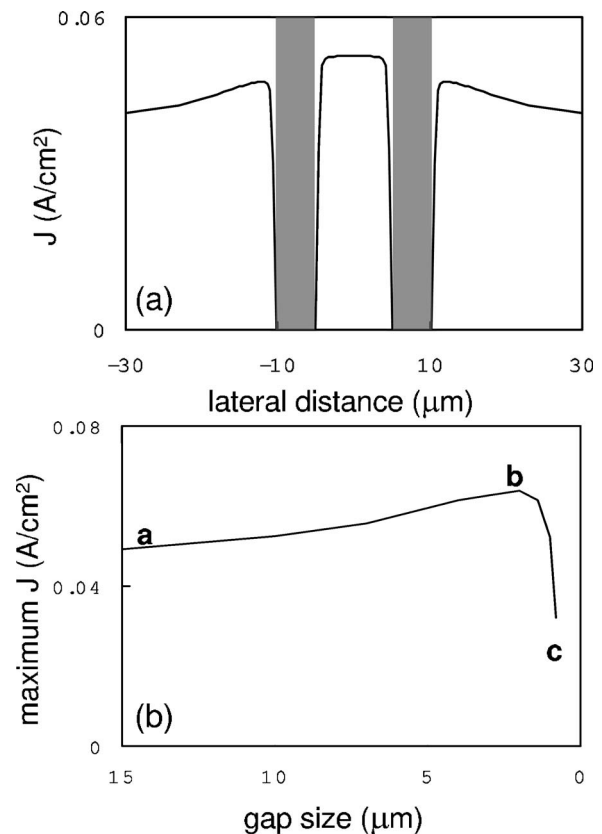

FIG. 6. (a) MEDICI plot of J across a region comprising two 5-μm-wide irradiated lines with a 10-μm gap. The background level, far from the irradiated structure, is J=40 mA/cm^2. (b) Maximum J in the gap as a function of gap size.

IV. MULTIPLE-LINE IRRADIATIONS

Here J in and around structures comprising two or more line irradiations are considered. In Fig. 6(a), J is highest in the gap; immediately outside the structure, J is also high and gradually reduces towards the background level. Figure 6(b) plots the maximum J in the gap as a function of gap size. J rises above the background level for gaps larger than ~2 μm and rapidly reduces towards zero for smaller gaps.

This is explained in Fig. 7, where the resultant **E**-field lines (i.e., the sum of all the **E**-field vectors) during anodization are plotted for different gaps. In Fig. 7(a) those **E**-field lines deflected away from the irradiated lines are equally divided to either side. The higher **E** field produced in, and adjacent to, the large gap increases J above the background level. In Fig. 7(b) the same **E**-field lines deflected into the smaller gap produce a higher **E** field and a maximum J. In Fig. 7(c), **E**-field lines are more likely to be excluded from the small gap. This can be understood from Fig. 4 where the lateral **E** field extends up to 1 μm away from an irradiated line; the hole current flowing towards two such lines separated by <2 μm is deflected outside them, leading to a reduction of J.

Figure 8 plots J across a structure comprising ten irradiated lines for four proton doses. In the gaps and adjacent to the whole structure, J progressively increases above the background with increasing dose, while J through the irradi-
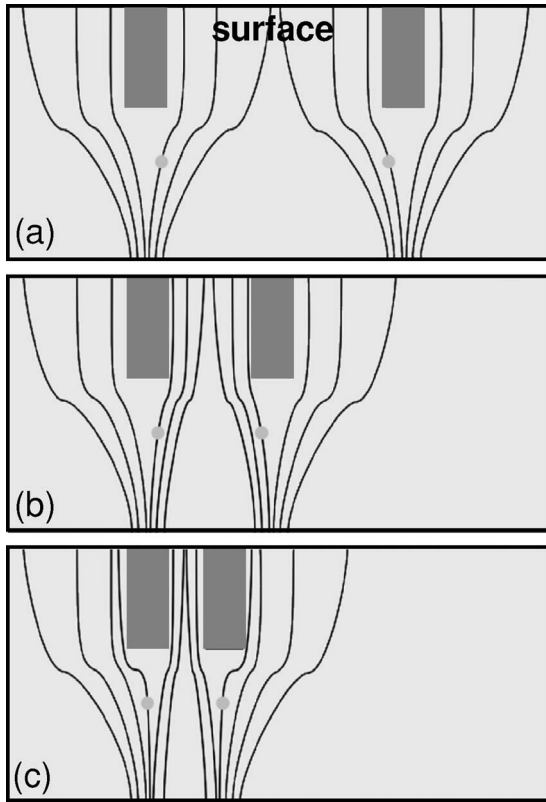
FIG. 7. Schematic of the **E**-field lines around two irradiated lines with decreasing gap size. Note the behavior of the dotted **E**-field line, which moves from inside to outside the gap with decreasing gap size.

ated lines decreases. In all simulations for such structures the gap size at which J is a maximum depends on the ion type, energy, and dose as well as the irradiated-line width, but the general behavior is always similar to that in Figs. 6 and 8. In general, J in the gaps is above the background level for large gaps and high doses and below it for small gaps.

Figures 9 and 10 exhibit many aspects of the behavior predicted above. In Fig. 9 the irradiated lines are all 5 μm wide and the gaps range from 10 μm to 1.5 μm. The large gaps are fully etched in Figs. 9(a) and 9(b); i.e., all silicon between the irradiated lines is removed because J is greater
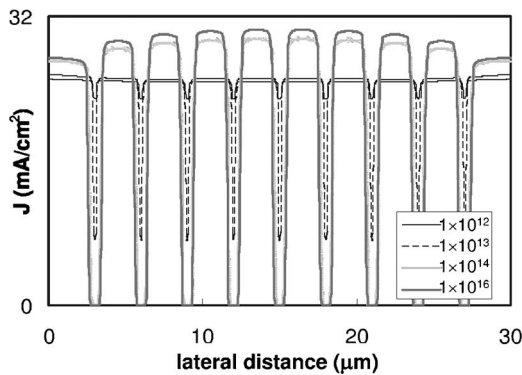

FIG. 8. MEDICI plot of J across a region comprising ten 0.5-μm-wide irradiated lines in a $3-\Omega$ cm wafer, separated by gaps of 2.5 μm, for four proton doses/cm^2.
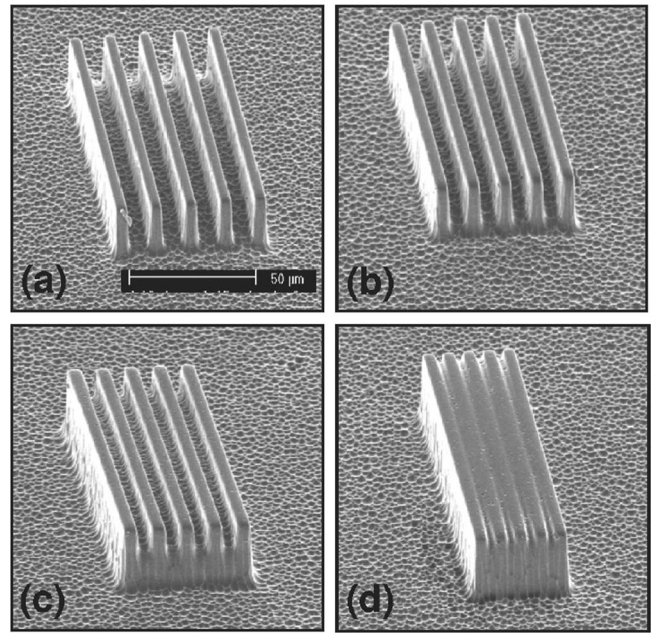

FIG. 9. SEM images of proton irradiated lines in a $3-\Omega$ cm wafer, all 5 μm wide, separated by gaps of (a) 10 μm, (b) 5 μm, (c) 2.5 μm, and (d) 1.5 μm. Dose of 10^{15}/cm^2, etched at J =100 mA/cm^2 for 5 min, then PSi removed.

than or equal to the background level during anodization. The gaps become less etched in Figs. 9(c) and 9(d) as the gap size reduces, since J decreases below the background level.

In Fig. 10, ten 200-nm-wide lines were irradiated with different gaps and doses. In Fig. 10(a) the gap is 7 μm and the irradiation dose for each line increases from right to left.
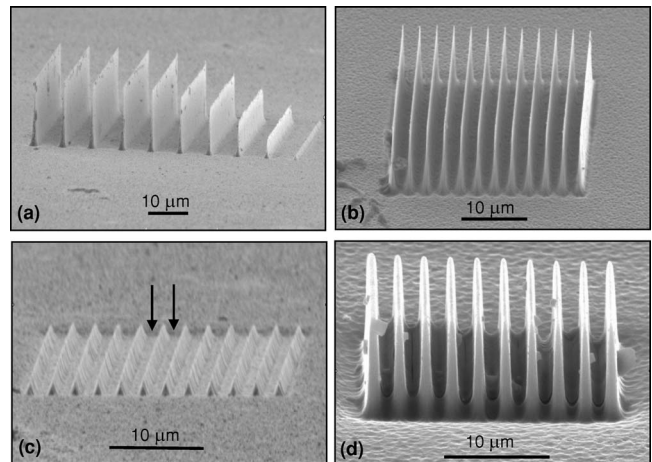

FIG. 10. SEM images of structures comprising ten irradiated lines. (a) $0.3-\Omega$ cm wafer with a gap of 7 μm and a dose linearly increasing from 1×10^{15} to 1×10^{16}/cm^2 from right to left. (b) $0.3-\Omega$ cm wafer with a gap of 2 μm and a dose of 5×10^{15}/cm^2. (c) $0.3-\Omega$ cm wafer with a gap of 3.5 μm and a dose of 1.8 $\times 10^{15}$/cm^2. The arrows point to the lower surface in the gaps compared to the background. (d) $3-\Omega$ cm wafer, with a gap of 2.5 μm and a dose of 1×10^{16}/cm^2. (a)–(c) were etched at J =100 mA/cm^2 for 5 min; (d) was etched at J=20 mA/cm^2 for 15 minutes.
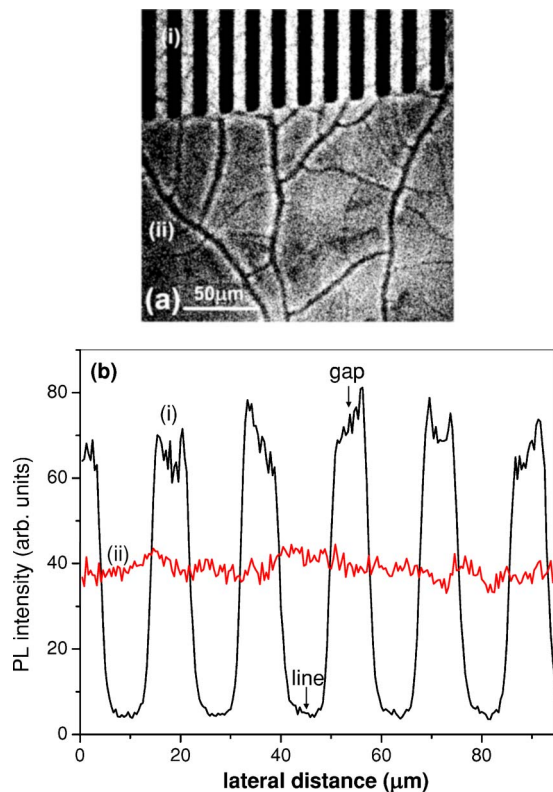
FIG. 11. (Color online) (a) PL image showing intensity variations across a structure comprising 20 irradiated vertical lines, in the upper portion of the image, which are 10 μm wide and separated by 5-μm gaps, in a $3-\Omega$ cm wafer. White and dark regions, respectively, correspond to areas of high and low measured PL intensity. The dose was 5×10^{14}/cm^2 and PL was excited with a 405-nm laser in a confocal microscope. (b) Horizontal line scans extracted from (a), plotting PL intensity across (i) the irradiated lines and gaps and (ii) the unirradiated background.

At low doses, the irradiated lines are partially etched, since J flowing through them is still significant [Fig. 3(a)]. At an optimum dose of 5×10^{15}/cm^2 the irradiated lines are unetched, since J flowing through them is reduced to zero. This optimum dose was used in Fig. 10(b); even though the gaps are only 2 μm, they are fully etched since J remains large because the dose is not large enough to exclude **E**-field lines from the gaps (Fig. 7). The irradiated lines are only $\sim$200 nm wide at the top, equal to the beam spot size, and they broaden with depth due to the lateral spreading [Fig. 2(a)]. A lower dose of 1.8×10^{15}/cm^2 was used in Fig. 10(c)

so the irradiated lines are significantly etched. It can be observed here that the gaps are etched significantly more than the background level, consistent with J being higher than the background.

It was predicted that narrow features are more difficult to produce in higher-resistivity material, since the optimum dose where J is reduced to zero is smaller, hence harder to find experimentally. Figure 10(d) shows a structure similar to Fig. 10(b), but created in a higher-resistivity wafer. Even in this, the most successful of our attempts, the irradiated lines are still $\sim$800 nm wide, since the lateral **E** field around them is strong (Fig. 4) and incomplete etching occurs in the small gaps, where J is less than the background level. Figure 5(d) shows a similar example where incomplete etching occurs in small gaps between point irradiations which are too close together. The pillars are only partially etched since J over the central irradiated areas is significantly reduced. The pillars closer to the edges of the irradiated area are more etched, since J at the edges is larger.

When J in the gaps is higher than the background level, the higher etch rate results in the gaps being etched deeper than the background level in Fig. 10(c). Whether this also produces measurably different PL properties of the PSi layer in the gaps is now considered. Figure 11 shows a PL image of 20 vertical irradiated lines and horizontal line scans extracted from it. The irradiated lines emit little PL due to the large irradiation dose. In the gaps where J is large, PL is emitted which is twice as bright as the background level. This may be attributed to the PSi layer in the gaps being thicker, in addition to the porosity increasing with J, resulting in stronger quantum confinement effects by the smaller silicon nanoparticles.[15,16]

V. CONCLUSIONS

The effects of focused MeV proton beam irradiation on porous silicon formation in electrochemically anodized wafers has been characterized and many aspects of the simulated behavior have been observed in SEM and PL images. The irradiation dose is more critical than the end-of-range beam spreading in determining the minimum lateral feature resolution. Feature sizes of $\sim$200 nm have been produced with an optimum irradiation dose. The current density between irradiated areas may either rise above the background level or fall to zero, depending on the irradiation geometry, wafer resistivity, and irradiation dose.

[1] L. T. Canham, Appl. Phys. Lett. **57**, 1046 (1990).

[2] L. T. Canham, Phys. World **5**, 41 (1992).

[3] A. G. Cullis, L. T. Canham, and P. D. J. Calcott, J. Appl. Phys. **82**, 909 (1997).

[4] S. Ossicini, L. Pavesi, and F. Priolo, *Light Emitting Silicon for Microphotonics*, Vol. 194 of *Springer Tracts in Modern Physics* (Springer-Verlag, Berlin, 2003), p. 75.

[5] K. D. Hirschman, L. Tsybeskov, S. P. Duttagupta, and P. M.

Fauchet, Nature (London) **384**, 338 (1996).

[6] J. C. Barbour, D. Dimos, T. R. Guilinger, M. J. Kelly, and S. S. Tsao, Appl. Phys. Lett. **59**, 2088 (1991).

[7] Xi-Mao Bao and Hai Qiang Yang, Appl. Phys. Lett. **63**, 2246 (1993).

[8] J. Xu and A. J. Steckl, Appl. Phys. Lett. **65**, 2081 (1994).

[9] P. Schmuki, L. E. Erickson, and D. J. Lockwood, Phys. Rev. Lett. **80**, 4060 (1998).

[10] L. Pavesi, G. Giebel, F. Ziglio, G. Mariotto, F. Priolo, S. U. Campisano, and C. Spinella, Appl. Phys. Lett. **65**, 2182 (1994).

[11] M. B. H. Breese, D. N. Jamieson, and P. J. C. King, *Materials Analysis using a Nuclear Microprobe* (Wiley, New York, 1996).

[12] J. A. van Kan, A. A. Bettiol, and F. Watt, Appl. Phys. Lett. **83**, 1629 (2003).

[13] E. J. Teo, D. Mangaiyarkarasi, M. B. H. Breese, A. A. Bettiol, and D. J. Blackwood, Appl. Phys. Lett. **85**, 4370 (2004).

[14] D. Mangaiyarkarasi, E. J. Teo, M. B. H. Breese, A. A. Bettiol, and D. J. Blackwood, J. Electrochem. Soc. **152**, D173 (2005).

[15] E. J. Teo, M. B. H. Breese, A. A. Bettiol, D. Mangaiyarkarasi, F. J. T. Champeaux, F. Watt, and D. J. Blackwood, Adv. Mater. **18**, 51 (2006).

[16] V. Lehmann, *Electrochemistry of Silicon* (Wiley-VCH, Weinheim, 2002).

[17] E. J. Teo, M. B. H. Breese, E. P. Tavernier, A. A. Bettiol, F. Watt, M. H. Liu, and D. J. Blackwood, Appl. Phys. Lett. **84**, 3202 (2004).

[18] E. J. Teo, E. P. Tavernier, M. B. H. Breese, A. A. Bettiol, and F. Watt, Nucl. Instrum. Methods Phys. Res. B **222**, 513 (2004).

[19] H. G. Craighead, Science **290**, 1532 (2000).

[20] A. N. Cleland and M. L. Roukes, Appl. Phys. Lett. **69**, 2653 (1996).

[21] J. Fritz, M. K. Baller, H. P. Lang, H. Rothuizen, P. Vettiger, E. Meyer, H.-J. Guntherodt, Ch. Gerver, and J. K. Gimzewski, Science **288**, 316 (2000).

[22] S. Y. Lin, J. G. Fleming, D. L. Hetherington, B. K. Smith, R. Biswas, K. M. Ho, M. M. Sigalas, W. Zubrzycki, S. R. Kurtz, and J. Bur, Nature (London) **394**, 251 (1998).

[23] J. F. Ziegler, J. P. Biersack, and U. Littmark, *The Stopping and Range of Ions in Solids* (Pergamon Press, New York, 2003).

[24] B. G. Svensson, B. Mohadjeri, A. Hallen, J. H. Svensson, and J. W. Corbett, Phys. Rev. B **43**, 2292 (1991).

[25] B. G. Svensson, C. Jagadish, A. Hallen, and J. Lalita, Nucl. Instrum. Methods Phys. Res. B **106**, 183 (1995).

[26] A. Hallen, N. Keskitalo, F. Masszi, and V. Nagi, J. Appl. Phys. **79**, 3906 (1996).

[27] M. Yamaguchi, S. J. Taylor, M. J. Yang, S. Matsuda, O. Kawasaki, and T. Hisamatsu, J. Appl. Phys. **80**, 4916 (1996).

[28] Synopsys Inc., TCAD Business Unit & Synopsys subsidiary, 2002, http://www.synopsys.com/.

[29] S. M. Sze, *Physics of Semiconductor Devices*, 2nd ed. (Wiley, New York, 1981).

[30] S. M. Hearne, Ph.D. thesis, The University of Melbourne, 2003.

[31] L. C. Feldman, J. W. Mayer, and S. T. Picraux, *Materials Analysis by Ion Channeling* (Academic, New York, 1982).